Electrical Power and Energy Systems 131 (2021) 107104

Contents lists available at ScienceDirect

International Journal of Electrical Power and Energy Systems

journal homepage: www.elsevier.com/locate/ijepes

Planning and reliability of DC microgrid configurations for Electric Vehicle Supply Infrastructure

B. Aluisio, M. Dicorato *, I. Ferrini, G. Forte, R. Sbrizzai, M. Trovato

Department of Electrical and Information Engineering, Politecnico di Bari, Bari, Italy

ARTICLE INFO

Keywords:
DC microgrid configurations
Electric vehicles
Converter selection
Optimal planning
Reliability analysis

ABSTRACT

Infrastructures for Electric Vehicle feeding, providing smart charging, vehicle-to-grid and local generation are of increasing interest. The operation of these systems and the integration with distribution networks can gain remarkable improvement by proper DC microgrid structure, able to reduce losses in converters, to improve controllability and to enhance overall availability. In this paper, a procedure for optimal planning of a DC microgrid for Electric Vehicle Supply Infrastructure is carried out, with specific tailoring according to technical configurations for source connection, involving different converter types and topologies. The procedure is completed by a reliability analysis, where rule-based curtailment is performed with multi-state matrix approach, and the effect of expected energy not supplied on total cost is evaluated, at different integration levels of energy storage. The proposed approach is applied to a case study of envisaged demonstrator for an Electric Vehicle service fleet.

1. Introduction

In order to underpin the diffusion of Electric Vehicles (EVs), their proper management is required for reducing possible malfunctioning of distribution systems. In this framework, the integration in microgrids would be beneficial, exploiting local intelligence for optimal operation and control [1–3]. In particular, the integration of EV charging stations with energy storage system (ESS) and photovoltaic (PV) panels is suitable for parking-place shading systems [4–6]. In this way, an Electric Vehicle Supply Infrastructure (EVSI) can be set up, representing a modular realization for providing mobility and grid services based on microgrid structure [7].

The presence of native DC sources, such as PV systems and EV batteries, encourages the setup of DC microgrids, with a common DC link and able to manage the connection to AC low-voltage network of local distributor [8,9].

Further advantages of DC microgrids with respect to AC-based ones include higher robustness and efficiency due to DC converters, simpler control in the absence of frequency and reactive power, and increased reliability [10–12]; moreover, the vehicle-to-grid (V2G) option is easily supported in DC microgrid.

Several control schemes and architectures for DC microgrids have been synthesized in [13], whereas a specific DC infrastructure for EV with multiple connections to AC network is proposed in [14].

The investigation of reliability aspects in microgrid sizing, inspecting the influence of renewable and storage devices by means of different methods [15], has gained significant interest. In particular, the influence of reliability in microgrid operation cost by means of Expected Energy not Supplied (EENS) is faced in [16] through Markov chain model, and by means of Value of Loss Load (VOLL) applied to load curtailment in AC/DC microgrid in [17]. Moreover, an equivalent loss factor is exploited in [18] as a constraint for the optimal sizing problem. Reliability constraints based on loss of load expectation are adopted in [19] within a scenario analysis. Whereas, optimal design of microgrid involving reliability features is carried out in [20] with EENS and sensitivity studies, and in a two-stage problem in [21], involving Pareto curve and fuzzy logic to individuate the best solution. Optimal sizing of an islanded microgrid including different targets or constraints on costs and reliability is dealt with in [22]. In [23], a data mining technique is applied to a Monte-Carlo simulation in order to estimate the loss of load and islanding probability of a PV-based microgrid. In [24], scenarios

Abbreviations: AC, Alternating Current; DC, Direct Current; EEND, Expected Energy Not Delivered; EENS, Expected Energy Not Supplied; ESS, Energy Storage System; EV, Electric Vehicle; EVSI, Electric Vehicle Supply Infrastructure; LV, Low Voltage; MPPT, Maximum Power Point Tracking; MV, Medium Voltage; PCC, Point of Common Coupling; PV, Photovoltaic; SOC, State of Charge; V2G, Vehicle-to-Grid; VOLL, Value of Loss Load.

* Corresponding author.
E-mail address: maria.dicorato@poliba.it (M. Dicorato).

https://doi.org/10.1016/j.ijepes.2021.107104
Received 27 November 2019; Received in revised form 7 December 2020; Accepted 10 April 2021
Available online 30 April 2021

Nomenclature

EVSI sizing and operational planning

Indices (subscripts)

t	Time step
s	Scenario
p	PV technology
i	ESS technology
j	EV
k	EV station
r	Charging/V2G technology standard
m	PV converter
h	ESS converter
f	AC/DC grid connection converter
u	Three-port AC/DC/DC converter

Sets and general definitions

Nt	Total number of time steps
Ns	Total number of scenarios
Ωp	Set of available PV technologies (total number Np)
Ωi	Set of available ESS technologies (total number Ni)
Ωj	Set of EVs (total number Nj)
Ωk	Set of charging stations (total number Nk)
Ωr	Set of EV charging/V2G standards (total number Nr)
Ωm	Set of PV converters (total number Nm)
Ωh	Set of ESS converters (total number Nh)
Ωf	Set of AC/DC converters (total number Nf)
Ωu	Set of three-port converters (total number Nu)
Ny	Total number of years of the analysis
α	Discount rate
Δt	Duration of each time step [h]
D_s	Number of occurrences of the s-th scenario in a year

Cost breakdown

C_T	Total lifetime cost of the microgrid [€]
C_B	Total building cost of the microgrid [€]
C_B^P	Building cost of the PVs and their converters [€]
C_B^I	Building cost of the ESSs and their converters [€]
C_B^K	Building cost of the EV stations [€]
C_B^G	Building cost of DC microgrid internal connections and of AC network interface [€]
C_O	Total operation cost of the microgrid [€]

PV system parameters

ζ^M	PV converter efficiency
c_p	Investment cost of a PV panel of the p-th technology [€/kW]
c_m	Investment cost of the m-th PV converter [€]

Energy storage system parameters

ζ^H	ESS converter efficiency
c_i	Investment cost of an ESS module for the i-th technology [€/kWh]
c_h	Investment cost of the h-th ESS converter [€]
I_{sto}^{min}	Minimum ESS installation limit [kWh]

Electric vehicles and stations parameters

$\beta_{j,k,s}$	Binary value assigning the connection of the j-th EV at the k-th EV station in the s-th scenario
ζ^K	EV station efficiency
c_r	Investment cost in the r-th technology for vehicle charging/V2G station [€]

Grid connection parameters

W_f	Nominal power of the f-th AC/DC converter [kW]
ζ^F	AC/DC converter efficiency
W_u	Nominal power of the u-th three-port converter [kW]
ζ^U	Three-port converter efficiency
$\overline{P}^{\,g}$	Maximum exchangeable power at PCC, in either injection or withdrawal [kW]
c_f	Investment cost of the f-th AC/DC converter [€]
c_u	Investment cost of the u-th three-port converter [€]
c^G	Investment cost of converter-equipped PCC apparatus [€]
c^χ	Investment cost of synchronous PCC apparatus [€/kW]

Real State Variables

$P_{p,s,t}$	MPPT power production from p-th PV system at the t-th time step in the s-th scenario [kW]
$P_{s,t}^{w}$	Amount of power withdrawal from the distribution grid at the t-th time step in the s-th scenario [kW]
$P_{s,t}^{g}$	Amount of power injected into the distribution grid at the t-th time step in the s-th scenario [kW]
$P_{i,s,t}^{c}$	Charge power for the i-th ESS at the t-th time step in the s-th scenario [kW]
$P_{i,s,t}^{d}$	Discharge power for the i-th ESS at the t-th time step in the s-th scenario [kW]
$P_{j,s,t}^{c}$	Charge power for the j-th EV at the t-th time step in the s-th scenario [kW]
$P_{j,s,t}^{d}$	Discharge power for the j-th EV at the t-th time step in the s-th scenario [kW]
$P_{k,s,t}^{c}$	Total charge power at k-th EV station at the t-th time step in the s-th scenario [kW]
$P_{k,s,t}^{d}$	Total discharge power at k-th EV station at the t-th time step in the s-th scenario [kW]
$P_{f,s,t}^{w}$	Power withdrawal at AC side of f-th AC/DC converter at the t-th time step in the s-th scenario [kW]
$P_{f,s,t}^{g}$	Power injection from AC side of f-th AC/DC converter at the t-th time step in the s-th scenario [kW]
$P_{u,s,t}^{w}$	Power withdrawal at AC side of u-th three-port converter at the t-th time step in the s-th scenario [kW]
$P_{u,s,t}^{g}$	Power injection from AC side of u-th three-port converter at the t-th time step in the s-th scenario [kW]
R_p	Installed power for the p-th PV technology [kW]
R_i	Installed size for the i-th ESS technology [kWh]
R^F	Installed power for the AC/DC converter [kW]
R^U	Installed power for the three-port AC/DC converter [kW]
χ	Contractual power exchange level at PCC [kW]

Integer State Variables

$b_{r,k}$	Variable linking the k-th station to the r-th standard for charging/V2G it is equipped with
$b_{m,p}$	Binary variable indicating if the m-th PV converter is exploited for the p-th PV technology
$b_{h,i}$	Binary variable indicating if the i-th ESS converter is exploited for the i-th ESS technology
b_f	Binary variable to select the installation of the f-th AC/DC converter
b_u	Binary variable to select the installation of the u-th three-port converter

Reliability assessment

Indices (subscripts)

q	Internal components
z	Device
σ	Reliability state

Sets and general definitions

Nz	Total number of devices

$N\sigma$	Total number of reliability states
Quantities	
A_q	Availability of the q-th component
λ_q	Failure rate of the q-th component
$n_{q,z}$	Number of q-th components in the z-th device
A_z	Availability of the z-th device
U_z	Unavailability of the z-th device
λ_z	Failure rate of the z-th device
μ_z	Repair rate of the z-th device
$\nu_{\sigma,z}$	Binary availability condition status of the z-th device in the σ-th state
f_σ	Probability of occurrence of the σ-th state
π_σ	Success parameter the σ-th state
$P^{c}_{k,s,t,\sigma}$	Total charge power in the σ-th state at k-th EV station at the t-th time step of the s-th scenario [kW]
$P^{d}_{k,s,t,\sigma}$	Total discharge power in the σ-th state at k-th EV station at the t-th time step of the s-th scenario [kW]
$P^{c}_{j,s,t,\sigma}$	Charge power in the σ-th state for the j-th EV at the t-th time step in the s-th scenario [kW]
$P^{d}_{j,s,t,\sigma}$	Discharge power in the σ-th state for the j-th EV at the t-th time step in the s-th scenario [kW]
EENS	Expected energy not supplied over the operation year [kWh]
EEND	Expected energy not delivered over the operation year [kWh]
VOLL	Value of loss load [€/kWh]
C_R	Total reliability cost of the EVSI [€]

involving different renewable and EV user models in a microgrid are analysed with Monte-Carlo technique to obtain reliability indices. In [25], demand response and EV charge control, without V2G, are exploited in a procedure for evaluating reliability indices and EV charge failure rates, related to the lack of desired charge at parking leaving. Concerning grid integration, [26] investigates reliability of distribution network in the presence of EVs according to V2G time intervals.

Another field of research for microgrids involving EVs is the influence of ESS dimensioning and operation. In [27] ESS size for a parking lot is assessed according to EV charge stochastic behaviour and reduction techniques, determining EV tariff as well, whereas in [28] PV and ESS are dimensioned in a multi-agent framework considering known EV charge with queuing analysis; furthermore in [29] immediate, controlled and bidirectional EV charging are examined for microgrid operation under varying ESS sizes, in [30] the influence of energy price on optimal ESS power/capacity in a fast-charge station is assessed, and in [31] a Markov model of ESS charge/discharge and EV arrival/departure events is developed, accounting for target of outage probability for EV supply. The mutual influence of ESS sizing in EV charging station and distribution network is accounted in [32] considering different EV charge levels and grid reinforcement, whereas in [33] electric and road networks are considered in a problem of sizing and siting EV stations considering reliability check due to EV position. The ESS influence is investigated in home systems with EVs, such as in [34] analysing the impact of ESS installation cost and planning horizon, and in [35] in a sizing problem considering deterministic and stochastic EV behaviour.

From the literature analysis, it can be inferred that for microgrids involving EVs the aspects of optimal sizing and operation, of EV-oriented reliability evaluation and of ESS dimensioning have seldom been analysed in an organic way, especially considering the peculiarities of a DC-based architecture. In particular, the combination of these aspects in the assessment of alternative DC microgrid configurations has important implications on the planned investment and on the operation management in order to provide services to users or customers at defined levels.

In this paper, a procedure to assess sizing, operation and reliability of different DC-microgrid configurations for an EVSI is proposed. Four configurations are considered, involving appropriate combinations of converters as well as modular PV panels, ESS elements and EV charging stations, with a proper interface with the low-voltage AC distribution network. Taking the cue from the methodology carried out in [36], the procedure involves optimal installation and lifetime operation costs according to different conditions and EV needs. To this purpose, different exploitation levels of energy storage system are investigated. Moreover, a rule-based power curtailment method in the presence of device failures is adopted for the evaluation of reliability features, aimed at determining the expected levels of power exchange with EVs under different availability states, exploiting multi-state matrix approach [37]. The procedure is applied to the design of the test case for a DC microgrid

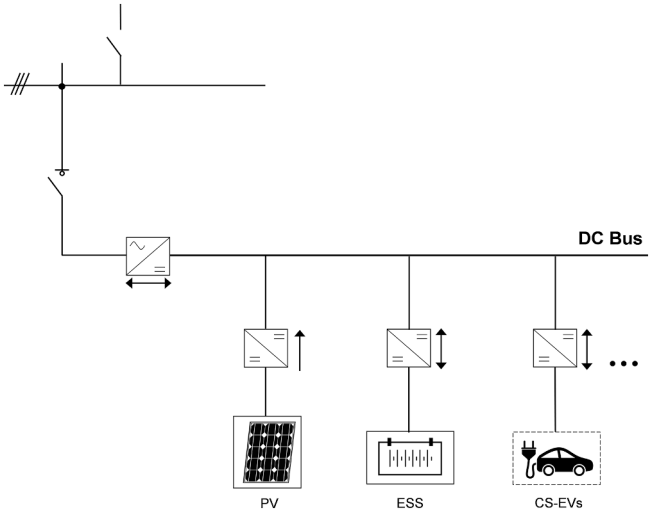

Fig. 1. Configuration A for the DC microgrid.

in the port area of Bari, Italy, considering the presence of a service fleet of EVs, and deriving proper reliability figures in terms of expected curtailed energy.

The main contributions of the paper can be individuated as follows:

- the procedure for DC microgrid optimal planning, involving sizing and operation, is improved, in order to account for the techno-economic peculiarities of different DC microgrid structures;
- proper reliability indices are obtained from the optimal planning by means of a rule-based curtailment in the presence of device unavailability;
- the influence of increasing ESS installation on microgrid operation and reliability is carried out;
- planning and reliability aspects are compared by proper costs, identifying levels of VOLL determining the convenience of ESS increase for each configuration.

The paper is organized as follows. Section 2 reports the proposed DC microgrid configuration and a description of converter main features. In Section 3, the formulation of the proposed methodology for DC microgrid optimal planning and operation is described, along with the method for the evaluation of reliability indices. In Section 4, the test case is presented and simulation results are illustrated and discussed. Conclusions are reported in Section 5.

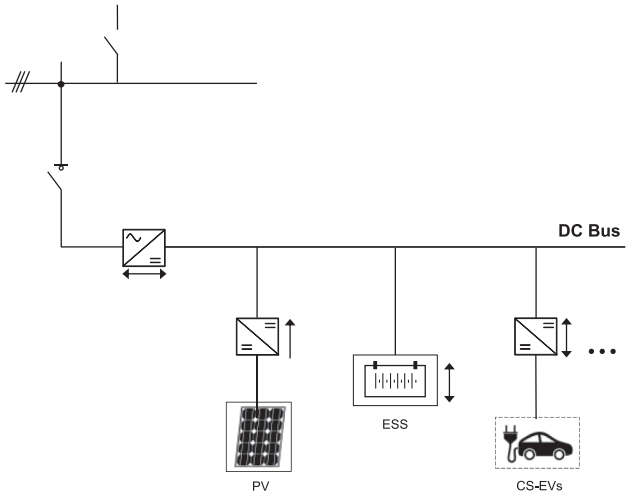

Fig. 2. Configuration B for the DC microgrid.

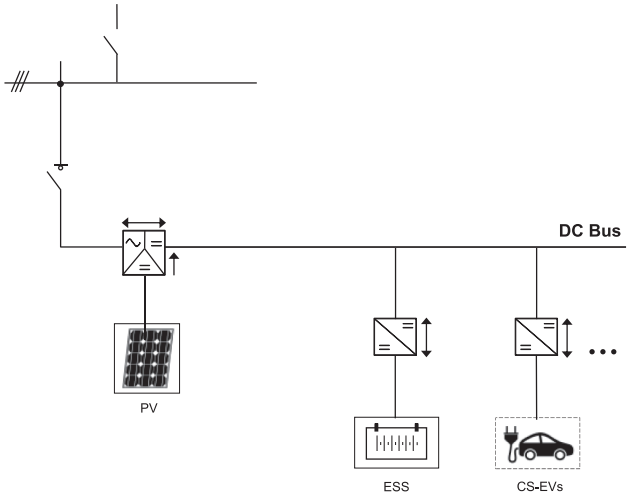

Fig. 3. Configuration C for the DC microgrid.

2. DC microgrid configurations and components

The following four configurations for DC microgrid of the EVSI are considered.

The Configuration A [11,36] is depicted in Fig. 1. It involves a bidirectional AC/DC converter for grid connection at Point of Common Coupling (PCC), a monodirectional DC/DC converter with maximum power point tracking (MPPT) functionality for the integration of PV system, a bidirectional DC/DC converter for the ESS and different bidirectional DC/DC converters for the EV charging stations, in order to enable V2G performances. All the converters, including relevant protection devices, are connected to a common DC busbar at proper voltage level. Moreover, suitable internal collection systems for the input of PV panel strings to the converter and for the ESS modules are provided.

Since the DC microgrid is less affected by voltage controllability concerns, different converterless schemes have been proposed in literature [38,39]. In Configuration B, direct ESS connection in DC microgrid is proposed, as reported in Fig. 2. In this case, the charge/discharge of the ESS will be driven by the relationship between DC bus voltage and ESS voltage, depending on its state of charge (SOC).

Further savings in converters can be achieved by the exploitation of three-port converters, able to manage PV and ESS on different DC ports and to interface either with AC or with DC circuit [40]. Due to the presence of multiple EV stations, the AC/DC/DC three-port converter is

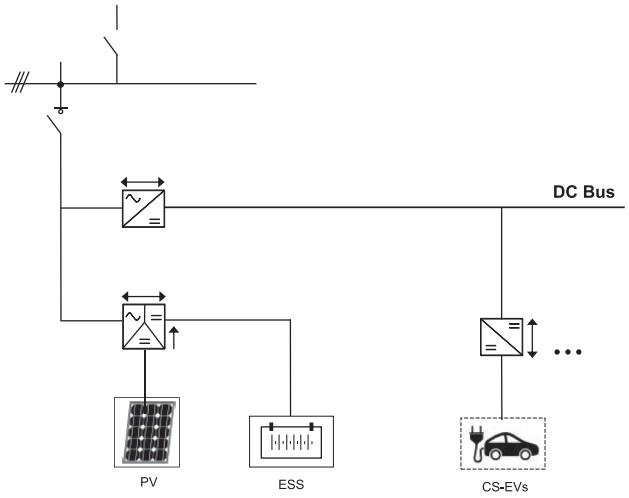

Fig. 4. Configuration D for the DC microgrid.

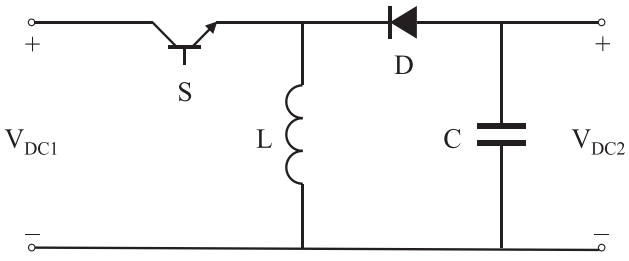

Fig. 5. DC/DC monodirectional buck-boost converter layout.

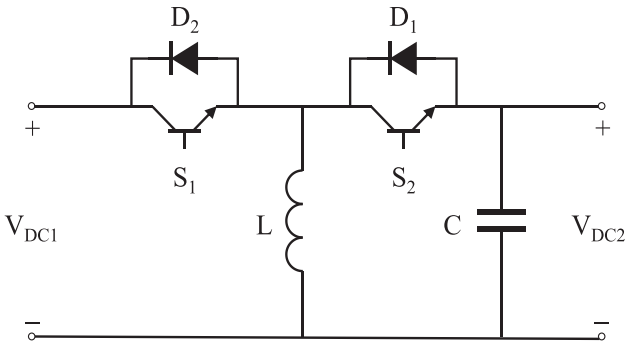

Fig. 6. DC/DC bidirectional buck-boost converter layout.

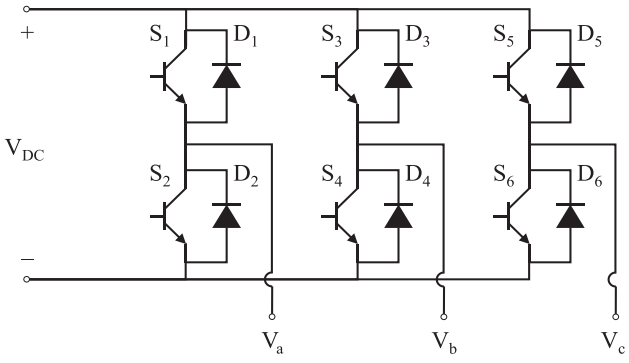

Fig. 7. Three-phase AC/DC bidirectional converter layout.

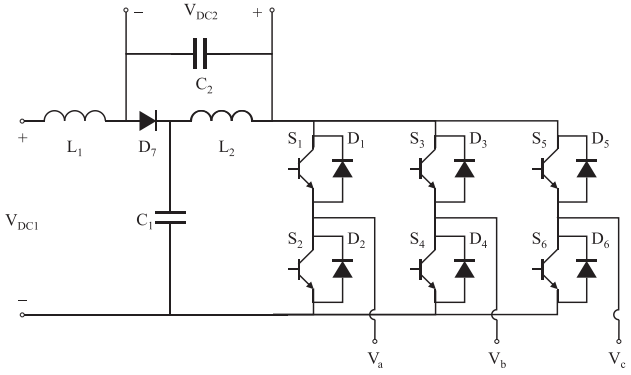

Fig. 8. AC/DC/DC three port converter layout.

selected for the proposed DC-based microgrid. In particular, it is exploited as interfacing device at PCC in Configuration C (see Fig. 3).

Moreover, in order to enhance flexibility and to derive a dedicated control on EV section, a hybrid scheme is proposed as Configuration D (see Fig. 4), exploiting the three-port AC/DC/DC converter for PV and ESS, and providing a distinct AC/DC bidirectional converter for the connection of the DC-busbar where all EV stations are linked.

For all the configurations, in grid-connected operation mode, the grid converter is supposed to behave as the master (voltage forming). Whereas, in the islanded mode, the master role is entrusted to the ESS (even with direct DC connection). PV and EVs are always slaves, and then controlled in active power. However, the synthesis of relevant controllers is beyond the scope of the paper.

In order to carry out the procedure for planning and reliability evaluation, standard transformerless layouts of DC/DC monodirectional and bidirectional converters, of AC/DC converter and of three-port AC/DC/DC converter are exploited, as reported in Figs. 5–8, based on current devices detected in a market survey. In particular, for DC/DC converters, buck-boost solutions are exploited since the ratio between the two DC voltage levels is not fixed. The AC sides are three-phase for proper connection to the distribution network. In these schemes, power transistors are named with S and diodes with D, whereas inductors and capacitors are indicated with L and C respectively, V_{DC} stands for DC-side voltage, whereas AC voltages are indicated with V. These names and relevant numeration are illustrative in order to determine component number for reliability analysis.

3. Planning and reliability evaluation methodology

The proposed methodology is composed of two main parts, performed for each DC microgrid configuration, developed and applied in a two-step open-loop framework.

At first, a procedure for optimal planning of the DC microgrid is applied. It is based on a mixed-integer linear programming problem, with the objective of reducing total lifetime microgrid costs C_T in the presence of proper constraints, as follows:

$$\begin{aligned} &minC_T(\boldsymbol{x}) \\ &\text{s.t.}\begin{cases} g(\boldsymbol{x}) = 0 \\ h(\boldsymbol{x}) \leqslant 0 \\ \underline{\boldsymbol{x}} \leqslant \boldsymbol{x} \leqslant \overline{\boldsymbol{x}} \end{cases} \end{aligned} \tag{1}$$

The vector of state variables $\boldsymbol{x}$ includes installation levels of PV panels, ESS batteries, EV charging/V2G stations, as well as PV power production, ESS charge/discharge power, EV charge/discharge power and grid power withdrawal/delivery in each of the *Nt* time steps for a set of *Ns* scenarios (corresponding to sample days of operation), defined according to EV exploitation for mobility and weather conditions. Moreover, integer state variables include binary variables for choosing proper technologies and sizes of converters, as well as for distinguishing charge/discharge processes.

The procedure involves the analysis of *Np* PV systems, *Ni* ESSs, *Nj* EVs,*Nk* stations exploiting *Nr* standards for charging or V2G. The models of different components within the EVSI (PV production, ESS state, EV connections and state) are described in [36], where optimal planning of Configuration A has been investigated, along with a procedure for the commitment of EVs and charging stations. The general optimization procedure explicated in [36] is tailored and applied to the different configurations under investigation, as described in Section 3.1.

Once the optimal sizing and planning is obtained, and the operation conditions of each device in each time step of each scenario are assessed, the reliability evaluation is developed, aiming to determine the reduction of energy exchange with EVs, either charging or discharging, that can occur in the presence of device unavailability, weighed according to probability of occurrence, determined through failure rates analysis, and exploiting a rule-based curtailment method, with the final evaluation of reliability cost. The description of reliability evaluation procedure is provided in Section 3.2.

3.1. Microgrid optimal planning: peculiarities of DC microgrid configurations

Charge and discharge power of the *j*-th EV in the *t*-th time step of the *s*-th scenario are defined as $P^{c}_{j,s,t}$ and $P^{d}_{j,s,t}$ respectively, and $\beta_{j,k,s}$ is a binary parameter assigning the connection of the *j*-th EV at the *k*-th station in the *s*-th scenario, obtained from EV station commitment procedure. Therefore, the power exchange at the *k*-th EV station in the *t*-th time step of the *s*-th scenario, defined as $P^{c}_{k,s,t}$ if in charge and $P^{d}_{k,s,t}$ if in discharge, is obtained as follows:

$$P^{c}_{k,s,t} = \sum_{j=1}^{Nj} P^{c}_{j,s,t} \cdot \beta_{j,k,s} \tag{2.a}$$

$$P^{d}_{k,s,t} = \sum_{j=1}^{Nj} P^{d}_{j,s,t} \cdot \beta_{j,k,s} \tag{2.b}$$

The main differences among the configurations described in Section 2 lie in microgrid power balance, in connection with external AC network and in the definition of the cost function.

3.1.1. Microgrid power balance

Power balance at the *t*-th time step of the *s*-th scenario in Configuration A is described by the following relation, where the left-side term refers to power generation and the right-side term concerns power consumption:

$$\begin{aligned} &\zeta^{M} \cdot \sum_{p=1}^{Np} P_{p,s,t} + \zeta^{H} \cdot \sum_{i=1}^{Ni} P^{d}_{i,s,t} + \zeta^{K} \cdot \sum_{k=1}^{Nk} P^{d}_{k,s,t} + \zeta^{F} \cdot P^{w}_{s,t} \\ &= \frac{1}{\zeta^{H}} \cdot \sum_{i=1}^{Ni} P^{c}_{i,s,t} + \frac{1}{\zeta^{K}} \cdot \sum_{k=1}^{Nk} P^{c}_{k,s,t} + \frac{1}{\zeta^{F}} \cdot P^{g}_{s,t} \end{aligned} \tag{3.a}$$

For Configuration B, the ESS converter efficiency is not present, therefore the power balance assumes the following expression:

$$\zeta^M \cdot \sum_{p=1}^{Np} P_{p,s,t} + \sum_{i=1}^{Ni} P^{d}_{i,s,t} + \zeta^K \cdot \sum_{k=1}^{Nk} P^{d}_{k,s,t} + \zeta^F \cdot P^{w}_{s,t} = \sum_{i=1}^{Ni} P^{c}_{i,s,t} + \frac{1}{\zeta^K} \cdot \sum_{k=1}^{Nk} P^{c}_{k,s,t} + \frac{1}{\zeta^F} \cdot P^{g}_{s,t} \quad (3.b)$$

In Configuration C, the three-port converter efficiency ζ^U is applied to PV and grid connection, and the following relation is obtained:

$$\zeta^U \cdot \sum_{p=1}^{Np} P_{p,s,t} + \zeta^H \cdot \sum_{i=1}^{Ni} P^{d}_{i,s,t} + \zeta^K \cdot \sum_{k=1}^{Nk} P^{d}_{k,s,t} + \zeta^U \cdot P^{w}_{s,t} = \frac{1}{\zeta^H} \cdot \sum_{i=1}^{Ni} P^{c}_{i,s,t} + \frac{1}{\zeta^K} \cdot \sum_{k=1}^{Nk} P^{c}_{k,s,t} + \frac{1}{\zeta^U} \cdot P^{g}_{s,t} \quad (3.c)$$

For Configuration D, three balance equations are imposed, as follows:

$$\zeta^K \cdot \sum_{k=1}^{Nk} P^{d}_{k,s,t} + \zeta^F \cdot P^{w}_{f,s,t} = \frac{1}{\zeta^K} \cdot \sum_{k=1}^{Nk} P^{c}_{k,s,t} + \frac{1}{\zeta^F} \cdot P^{g}_{f,s,t} \quad (3.d)$$

$$\sum_{p=1}^{Np} P_{p,s,t} + \sum_{i=1}^{Ni} P^{d}_{i,s,t} + \zeta^U \cdot P^{w}_{u,s,t} = \sum_{i=1}^{Ni} P^{c}_{i,s,t} + \frac{1}{\zeta^U} \cdot P^{g}_{u,s,t} \quad (3.e)$$

$$P^{w}_{s,t} - P^{g}_{s,t} = P^{w}_{u,s,t} - P^{g}_{u,s,t} + P^{w}_{f,s,t} - P^{g}_{f,s,t} \quad (3.f)$$

In particular, (3.d) represents the power balance at DC node of EV stations, (3.e) at DC node of the three-port converter, and (3.f) at AC collection node for grid connection.

3.1.2. Connection with AC network

The power exchange across the interfacing grid converter should withstand specific constraints. For the installed converter size, the following relations are valid for the AC/DC two-port converter, present in Configurations A, B, D:

$$R^F = \sum_{f \in \Omega f} W_f \cdot b_f \quad (4.a)$$

$$\sum_{f \in \Omega f} b_f = 1 \quad (4.b)$$

In particular, (4.a) relates the installed power to the selected size, and (4.b) ensures that only one size is selected.

Analogously, for the three-port converter, the following constraints can be imposed:

$$R^U = \sum_{u \in \Omega u} W_u \cdot b_u \quad (5.a)$$

$$\sum_{u \in \Omega u} b_u = 1 \quad (5.b)$$

Moreover, grid exchange levels are bounded by installed converter size, therefore for Configurations A and B the following relations hold:

$$0 \leqslant P^{g}_{s,t} \leqslant R^F \quad (6.a)$$

$$0 \leqslant P^{w}_{s,t} \leqslant R^F \quad (6.b)$$

In order to make maximum power exchange levels explicit, the contractual grid power exchange is introduced. For Configurations A and B, it can be argued that

$$\chi = R^F \quad (6.c)$$

In the case of Configuration C, the grid exchange levels are bounded by three-port converter installed size. Therefore, the following constraints are placed:

$$0 \leqslant P^{g}_{s,t} \leqslant R^U \quad (7.a)$$

$$0 \leqslant P^{w}_{s,t} \leqslant R^U \quad (7.b)$$

$$0 \leqslant \sum_{p=1}^{Np} P_{p,s,t} \leqslant R^U \quad (7.c)$$

$$\chi = R^U \quad (7.d)$$

In particular, (7.c) links PV power production to three-port converter installed size.

In Configuration D, features of two-port and three-port converters have to be taken into account. In particular, for two-port converter, the following relations are valid:

$$0 \leqslant P^{g}_{f,s,t} \leqslant R^F \quad (8.a)$$

$$0 \leqslant P^{w}_{f,s,t} \leqslant R^F \quad (8.b)$$

$$0 \leqslant P^{g}_{f,s,t} \leqslant \overline{P}^{g} \cdot b_f \quad (8.c)$$

$$0 \leqslant P^{w}_{f,s,t} \leqslant \overline{P}^{g} \cdot \left(1 - b_f\right) \quad (8.d)$$

where (8.a)–(8.b) represent power exchange limits and (8.c)–(8.d) ensure power flowing in one direction per time interval. Analogously, for three-port converter, the following constraints are placed:

$$0 \leqslant P^{g}_{u,s,t} \leqslant R^U \quad (9.a)$$

$$0 \leqslant P^{w}_{u,s,t} \leqslant R^U \quad (9.b)$$

$$0 \leqslant \sum_{p=1}^{Np} P_{p,s,t} \leqslant R^U \quad (9.c)$$

$$0 \leqslant \sum_{i=1}^{Ni} P^{c}_{i,s,t} \leqslant R^U \quad (9.d)$$

$$0 \leqslant \sum_{i=1}^{Ni} P^{d}_{i,s,t} \leqslant R^U \quad (9.e)$$

$$0 \leqslant P^{g}_{u,s,t} \leqslant \overline{P}^{g} \cdot b_u \quad (9.f)$$

$$0 \leqslant P^{w}_{u,s,t} \leqslant \overline{P}^{g} \cdot \left(1 - b_u\right) \quad (9.g)$$

where (9.a)–(9.b) impose limits on power exchange at AC side, (9.c)–(9.e) are DC-sides limits for PV and ESS, and (9.f)–(9.g) avoid contemporaneous bidirectional flows on AC connection.

Eventually, the following constraints regulate the power exchange with the external AC network and allow to define the contractual power exchange:

$$0 \leqslant P^{g}_{s,t} \leqslant \chi \quad (10.a)$$

$$0 \leqslant P^{w}_{s,t} \leqslant \chi \quad (10.b)$$

3.1.3. Minimum ESS installation

In order to ensure proper microgrid operation in the islanded mode and to inspect the effectiveness of energy storage, a minimum limit to global ESS installation is added to problem constraints, as follows:

$$\sum_{i=1}^{Ni} R_i \geqslant I^{min}_{sto} \quad (11)$$

3.1.4. Cost function

The total lifetime cost C_T of the EVSI is given by the sum of construction cost C_B and lifetime operation cost C_O. While the latter is given

by the actualization of total yearly operation costs, involving grid exchange and EV charge/discharge [36], the former is given by the sum of installation costs for PVs, for ESSs, for EV stations and for grid connection C_B^G. The first three terms are expressed as follows:

$$C_B^P = \sum_{p=1}^{Np}\left(c_p \cdot R_p + \sum_{m\in\Omega m} c_m \cdot b_{m,p}\right) \tag{12.a}$$

$$C_B^I = \sum_{i=1}^{Ni}\left(c_i \cdot R_i + \sum_{h\in\Omega h} c_h \cdot b_{h,i}\right) \tag{12.b}$$

$$C_B^K = \sum_{r=1}^{Nr} c_r \cdot \sum_{k=1}^{Nk} b_{r,k} \tag{12.c}$$

It should be noted that in Configuration B $b_{h,i} = 0$ due to the absence of ESS converter, whereas in Configuration C $b_{m,p} = 0$ since PV is interfaced by three-port converter. In Configuration D, the three-port converter connecting PV and ESS implies both $b_{h,i} = 0$ and $b_{m,p} = 0$.

The installation cost of grid connection C_B^G in Configurations A and B includes AC/DC converter and converter-equipped PCC apparatus, as follows:

$$C_B^G = \sum_{f\in\Omega f}\left(c_f + c^G\right)\cdot b_f \tag{13.a}$$

Whereas, in Configuration C, the cost of three-port converter is accounted:

$$C_B^G = \sum_{u\in\Omega u}\left(c_u + c^G\right)\cdot b_u \tag{13.b}$$

For Configuration D, the evaluation includes both AC/DC and three-port converters including AC connection devices, considered analogous to converter-equipped PCC apparatus, along with contractual exchange with AC network, with a proper cost of synchronous PCC apparatus (not directly connected to a converter), as follows:

$$C_B^G = \sum_{f\in\Omega f}\left(c_f + c^G\right)\cdot b_f + \sum_{u\in\Omega u}\left(c_u + c^G\right)\cdot b_u + c^\chi \cdot \chi \tag{13.c}$$

3.2. Reliability assessment

Once the problem (1) is solved for each configuration, the relevant reliability is evaluated, by applying Markov chain for single devices and multi-state matrix approach for overall microgrid assessment.

As a first step, the failure rate and repair rate of each device z are determined, deriving the availability and unavailability of each device:

$$A_z = \mu_z/(\lambda_z + \mu_z) \tag{14.a}$$

$$U_z = \lambda_z/(\lambda_z + \mu_z) \tag{14.b}$$

The estimation of converter reliability indices is based on the failure rates of internal components λ_q (switches, diodes, filters, etc.) [41–43]. Each converter is assumed as a series system, therefore the device failure rate λ_z and device availability A_z can be determined as follows:

$$\lambda_z = \sum_q n_{q,z}\cdot\lambda_q \tag{15.a}$$

$$A_z = \prod_q n_{q,z}\cdot A_q \tag{15.b}$$

Whereas, for the main energy sources, proper values of failure rates λ_z are estimated, according to series and parallel connection of the modular components [44,45]. For instance, for the p-th PV system, the failure rate corresponds to the one of the most powerful string, given by the sum of failure rates of each panel of the string.

A set of system availability states $N\sigma = 2^{Nz}$ is built, including all the combinations of device availability, supposed independent on other devices. With these assumptions, the probability of occurrence of the σ-th state f_σ is given by:

$$f_\sigma = \prod_{z=1}^{Nz}\left[v_{\sigma,z}\cdot A_z + \left(1 - v_{\sigma,z}\right)\cdot U_z\right] \tag{16}$$

where $v_{\sigma,z}$ is equal to 1 if the z-th device is available in the σ-th state, and 0 otherwise.

Starting from the power exchange of each device obtained from the optimal planning procedure described in Section 3.1, the influence of the unavailability of any device in the σ-th state is evaluated for each time interval in each scenario by means of a rule-based power curtailment method according to sequential priorities of the devices in service, analogously to similar applications [46,47]. This is supposed to be the operation strategy of the whole system in the presence of any failure, and system reliability is assessed according to service not supplied to all the EVs. With these assumptions, EVs are considered always available when parked, analogously to assumptions in [26], although an estimation of specific reliability indicators for EVs could be carried out as indicated by [48].

The considered priorities are listed in Table 1, where the lowest the number, the highest the priority.

Table 1
Priority list of sources for reliability analysis.

Device in service	Device in failure			
	Grid	ESS	PV	EV stations
Grid	–	3	3	4
ESS	3	–	2	3
PV	2	2	–	2
EV stations	1	1	1	1

The priority list is applied only for the curtailment of non-zero quantities obtained in the operation stage of planning procedure, and no flow reversion is admitted. An exemplification of the method is reported in the general flowchart of Fig. 9, reporting the principles of all the possible combinations of Table 1. In particular, the residual exchange is determined as the pre-fault power exchange level of the faulty device in the considered condition, and the sequential curtailment is applied according to priority levels.

For instance, if in the σ-th state the external grid is unavailable, and in the t-th time step of the s-th scenario $P_{s,t}^{g} > 0$ (i.e., the EVSI is injecting power in the external grid at PCC), the power exchanges useful for curtailment are the ESS discharge, the PV production and the discharge of EV stations, in this order (see first column of Fig. 9). The method stops when the power balance is satisfied, i.e. residual exchange of the faulty device is nullified. In the opposite case of grid power withdrawal $P_{s,t}^{w} > 0$, the PV system is not involved, since it cannot increase the production from MPPT level exploited in the optimal planning (see second column of Fig. 9).

A detail of some example blocks of curtailment method is reported in Fig. 10.

For grid withdrawal reduction block (see Fig. 10.a) the following internal steps can be highlighted:

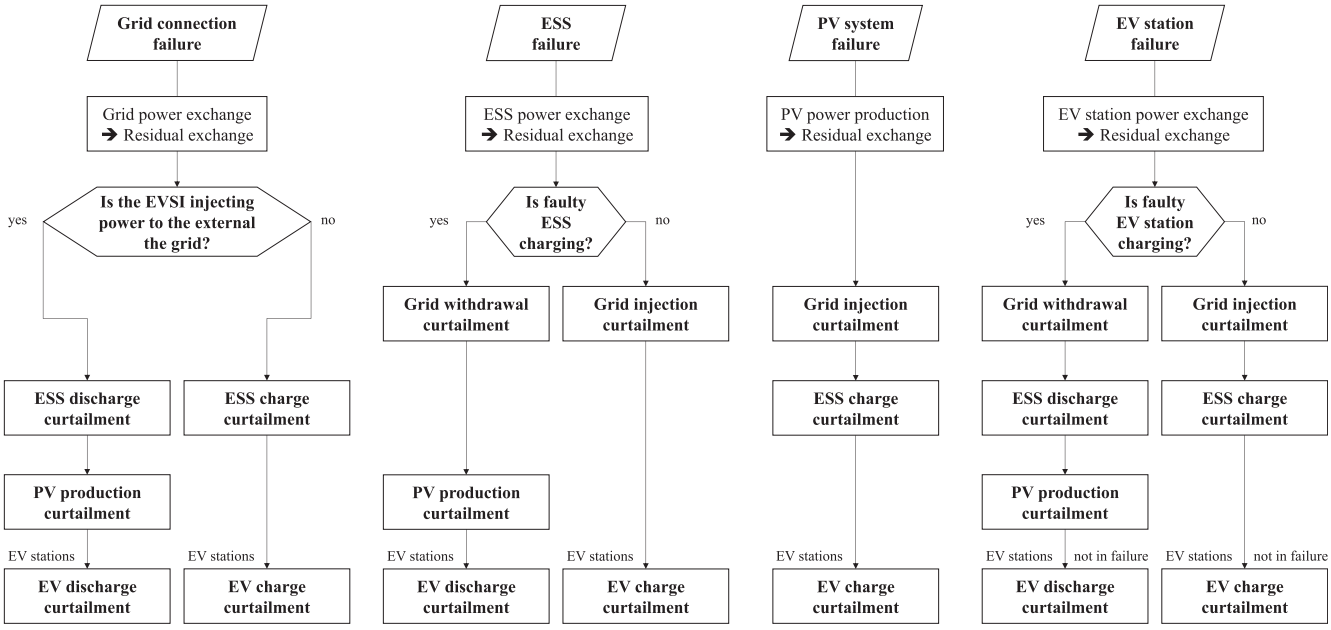

Fig. 9. General flowchart of rule-based curtailment method with priority levels.

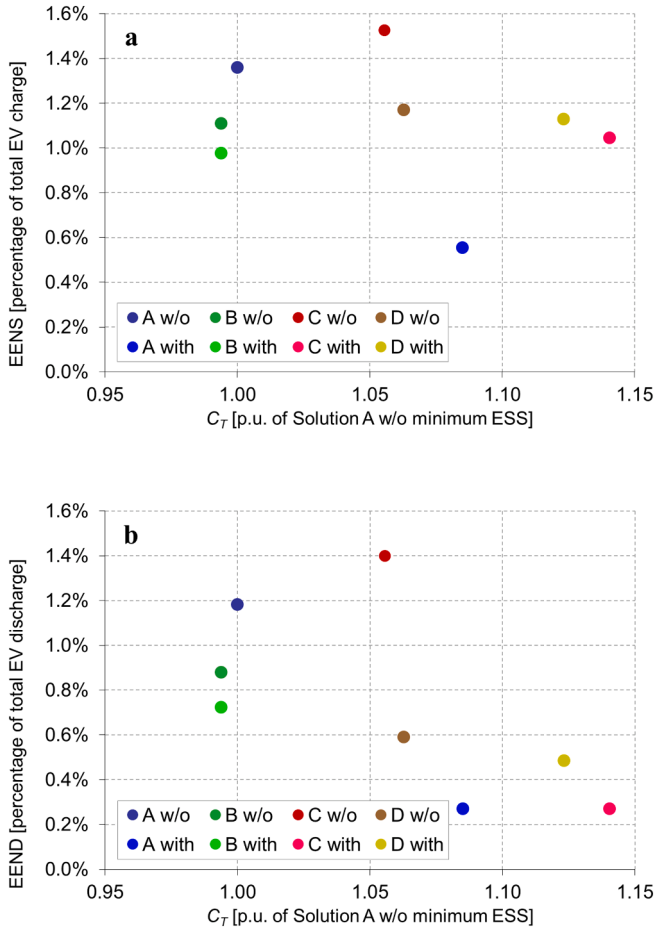

Fig. 10. Detailed description of example curtailment actions: grid withdrawal (a) and ESS discharge (b).

Table 2
Values of success parameter according to device availability in each state.

Device availability		Configuration			
Grid	ESS	A	B	C	D
Y	Y	1	1	1	1
Y	N	1	Depends on installed ESS	1	1
N	N	0	0	0	0

- if the EVSI was not draining power from the grid, the curtailment cannot be applied to the grid exchange, passing to the next priority level;
- if a grid withdrawal higher than zero is enough to nullify the residual exchange, it is applied and the method stops, without involving further priority levels; otherwise, new grid withdrawal level is set to zero and the residual exchange is updated, passing to the next priority level.

The same principles of grid withdrawal curtailment apply to grid injection and PV production.

For ESS discharge power reduction (see Fig. 10.b) the following internal steps can be highlighted:

- if the ESS was not discharging, the curtailment cannot be applied to the ESS, passing to the next priority level;
- the maximum reduction of ESS discharge implying a SOC level compatible with lower/upper bounds is determined (see [36], Eqs. (7) and (11));
- if a curtailment of ESS discharge down to maximum allowable reduction is enough to nullify the residual exchange, it is applied and the method stops, without involving further priority levels; otherwise, new ESS discharge is curtailed by maximum allowable reduction and the residual exchange is updated.

The same principles of ESS discharge curtailment apply to ESS charge and to EV stations, for charge and discharge, analyzing all stations not interested by fault.

In the presence of multiple failures, the power exchange of active devices is curtailed, following the priority list defined in Table 1, according to the net power exchange obtained in the planning procedure

Table 3
Optimal planning results.

			Configuration			
			A	**B**	**C**	**D**
Installation	PV polycr.	n	46	46	46	46
		kW	11.27	11.27	11.27	11.27
	ESS LiPo	n	0	2	0	1
		kWh	0	7.4	0	3.7
	EV Station 10 kW	n	5	5	5	5
	Grid connection	kW	10	10	20	20
	PV converter	kW	20	20	20	20
	ESS converter	kW	0	–	0	–
	Three-port converter	kW	–	–	20	20
	Two-port converter	kW	10	10	–	10
Energy production [kWh/y]	PV		15105.7	15105.7	15105.7	15105.7
	Grid withdrawal		1460.2	776.5	1510.7	993.4
	ESS discharge		0.0	2040.9	0.0	1137.6
	EV discharge		3290.9	2094.0	3283.7	2641.6
Energy consumption [kWh/y]	Grid injection		7134.7	6589.7	6735.2	6588.4
	ESS charge		0.0	2275.0	0.0	1261.0
	EV charge		11533.4	10084.8	11524.7	10747.6
Economic efforts [€]	C_T (**x**)		89933.4	89378.3	94963.6	95584.7
	C_B (**x**)		83483.6	84819.2	88186.2	90185.2
	C_O (**x**)		6449.8	4559.0	6750.4	5399.5
	Simulation time [s]		40.4	116.9	25.4	130.1

of all failing devices. In the case of failure of an EV station, the procedure reported in Appendix of [36] is applied to EVs planned to be parked at that station in order to try to find place in another free station during their whole parking time, and charge/discharge power could be modified according to station technology. If the EV does not find a free station, the planned power exchanges do not occur. All remaining EV stations could experience curtailments, if involved according to the priority list.

In the rule-based curtailment with priority, the assumption of keeping the direction of power exchange is aimed to ensure minimum deviation from the optimized program, evaluated in the planning procedure with fully available system and considering the whole daily horizon of each scenario. Moreover, the whole rule-based procedure allows to determine reliability conditions for each time interval, considering that device unavailability is expected to have limited duration and the same probability in any time interval, and to prevent zeroing of planned power exchange with EVs as much as possible.

Each availability state σ is further characterized by a success parameter π_σ, indicating the probability of the state to be sustained in actual operation, according to functioning principles of the active devices. The corresponding values for each configuration, reported in Table 2, depend on the availability of AC/DC grid converter and ESS, since they are in charge of master operation for the DC microgrid. In the case of grid availability, $\pi_\sigma = 1$ since system operation is ensured by voltage setting of grid converter. In the case of grid failure and ESS availability, $\pi_\sigma = 1$ for Configurations A, C and D, where a dedicated converter for ESS is present; whereas for Configuration B the value depends on installed ESS size, since DC microgrid voltage would be related to ESS state-of-charge and could easily fall outside operational limits of other converters if ESS size is limited. In the case of failure of both grid and ESS, the DC microgrid is shut off and $\pi_\sigma = 0$, since no voltage reference is applied and no power exchange can occur with EVs.

The rule-based curtailment procedure with priority gives out new amounts of power exchange across EV stations in the σ-th state in charge and in discharge, $P^{c}_{k,s,t,\sigma}$, $P^{d}_{k,s,t,\sigma}$ respectively. Finally, the charge/discharge power levels of each EV in the σ-th state, $P^{c}_{j,s,t,\sigma}$, $P^{d}_{j,s,t,\sigma}$, are obtained as follows:

$$P^{c}_{j,s,t,\sigma} = \sum_{k=1}^{Nk} P^{c}_{k,s,t,\sigma} \cdot \beta_{j,k,s} \tag{17.a}$$

$$P^{d}_{j,s,t,\sigma} = \sum_{k=1}^{Nk} P^{d}_{k,s,t,\sigma} \cdot \beta_{j,k,s} \tag{17.b}$$

Therefore, referring to EVs, values of *EENS* and *EEND* over the reference year with respect to the optimized program, evaluated in the planning procedure with fully available system, are derived as follows:

$$EENS = \sum_{\sigma=1}^{N\sigma} f_\sigma \cdot \sum_{s=1}^{Ns} D_s \cdot \sum_{j=1}^{Nj} \sum_{t=1}^{Nt} \left[\left(P^{c}_{j,s,t} - P^{c}_{j,s,t,\sigma} \right) \cdot \pi_\sigma + P^{c}_{j,s,t,\sigma} \cdot (1 - \pi_\sigma) \right] \tag{18.a}$$

$$EEND = \sum_{\sigma=1}^{N\sigma} f_\sigma \cdot \sum_{s=1}^{Ns} D_s \cdot \sum_{j=1}^{Nj} \sum_{t=1}^{Nt} \left[\left(P^{d}_{j,s,t} - P^{d}_{j,s,t,\sigma} \right) \cdot \pi_\sigma + P^{d}_{j,s,t,\sigma} \cdot (1 - \pi_\sigma) \right] \tag{18.b}$$

In (18.a)–(18.b), it can be noted that, if $\pi_\sigma = 1$, the rule based redispacthing is effective for the σ-th state, and the difference is estimated, whereas if $\pi_\sigma = 0$ all exchanged power is lost.

Finally, lifetime reliability cost C_R can be calculated by applying the *VOLL* to the *EENS*, and discounting the product by the annuity factor, as follows:

$$C_R = \frac{1 - (1 + \alpha)^{-Ny}}{\alpha} \cdot VOLL \cdot EENS \tag{19}$$

4. Test results

4.1. System under study

The procedure is applied to the envisaged realization of the DC-

Table 4
Optimal planning results with minimum ESS.

			Configuration			
			A	B	C	D
Installation	PV polycr.	n	46	46	46	46
		kW	11.27	11.27	11.27	11.27
	ESS LiPo	n	1	3	1	2
		kWh	3.7	11.1	3.7	7.4
	EV Station 10 kW	n	5	5	5	5
	Grid connection	kW	10	10	20	20
	PV converter	kW	20	20	20	30
	ESS converter	kW	10	–	10	–
	Three-port converter	kW	–	–	20	30
	Two-port converter	kW	10	10	–	10
Energy production [kWh/y]	PV		15105.7	15105.7	15105.7	15105.7
	Grid withdrawal		1086.9	689.1	1131.3	806.2
	ESS discharge		1021.5	2982.8	1019.3	2273.6
	EV discharge		2638.8	1466.8	2636.1	1819.6
Energy consumption [kWh/y]	Grid injection		6788.7	6581.3	6390.1	6752.2
	ESS charge		1138.7	3325.5	1136.0	2487.9
	EV charge		10744.2	9325.8	10741.0	9752.8
Economic efforts [€]	C_T (**x**)		97579.4	89379.3	102573.3	101020.6
	C_B (**x**)		92102.5	85466.7	96805.0	96732.7
	C_O (**x**)		5476.9	3912.6	5768.3	4287.9
	Simulation time [s]		144.5	24.5	38.7	113.8

Table 5
Equivalent devices in each configuration for reliability analysis.

	Number in Configuration				Reliability characteristics			
Equivalent device	**A**	**B**	**C**	**D**	λ_z [failure/h]	μ_z [repair/h]	A_z	U_z
External grid with AC/DC converter	1	1	0	0	$2.544{\cdot}10^{-5}$	$2.748{\cdot}10^{-3}$	0.99083	$9.173{\cdot}10^{-3}$
External grid	0	0	1	1	$4.110{\cdot}10^{-6}$	$5.708{\cdot}10^{-3}$	0.99928	$7.195{\cdot}10^{-4}$
PV system with DC/DC monodir. conv.	1	1	0	0	$3.421{\cdot}10^{-5}$	$7.915{\cdot}10^{-3}$	0.99570	$4.304{\cdot}10^{-3}$
PV system	0	0	1	1	$3.065{\cdot}10^{-5}$	$8.497{\cdot}10^{-3}$	0.99641	$3.594{\cdot}10^{-3}$
ESS system with DC/DC bidirect. conv.	1	0	1	0	$1.625{\cdot}10^{-5}$	$3.969{\cdot}10^{-3}$	0.99592	$4.077{\cdot}10^{-3}$
ESS system	0	1	0	1	$9.132{\cdot}10^{-6}$	$3.425{\cdot}10^{-3}$	0.99734	$2.660{\cdot}10^{-3}$
AC/DC/DC three-port converter	0	0	1	1	$2.138{\cdot}10^{-5}$	$2.0{\cdot}10^{-3}$	0.98942	$1.058{\cdot}10^{-2}$
AC/DC bidir. conv.	0	0	0	1	$7.117{\cdot}10^{-6}$	$5.0{\cdot}10^{-3}$	0.99858	$1.421{\cdot}10^{-3}$
EV charging station with DC/DC bidirect. conv.	5	5	5	5	$7.117{\cdot}10^{-6}$	$5.0{\cdot}10^{-3}$	0.99858	$1.421{\cdot}10^{-3}$

microgrid EVSI at Bari Port premises, with a fleet of 5 service EVs, usually exploited during the day for trips ranging between 20 and 100 km and parked at night. The investigated technologies include mono- and poly-crystalline for PV, LiPo, Zebra and Li-Ion batteries for ESS, and a set of discrete sizes for converters of PV, ESS and charging stations. Scenarios, spatial limits, weather data and tariffs are defined according to the previous work [36].

Moreover, for three-port converters in configurations C and D, nominal sizes W_u equal to 10, 20, 30 and 60 kW are analysed, considering converter efficiency $\zeta^U = 0.950$ [49] and installation cost $c_u = 350.0 \cdot W_u + 6675$ [€].

The cost for contractual AC network connection c^{χ} is fixed at 100 €/kW, according to average initial costs for connection in Italy.

4.2. Optimal planning application and results

The procedure is implemented in MatLAB2015b® framework, and solved by means of *intlinprog* function, exploiting branch and bound technique. Simulations are carried out on a workstation HP Z440 equipped with Intel Xeon 3.50 GHz processor with 16 GB RAM.

Installation and operation yields of optimal planning procedure for the four Configurations without minimum ESS installation (I_{sto}^{min}=0) are synthesized in Table 3. It can be observed that in Configurations A and C the ESS is not installed, due to the converter cost, and the EV discharge is more exploited with respect to Configurations B and D to cope with storage tasks. EV stations have the lowest nominal power due to long parking times. Total installation cost is lower in Configuration A due to the absence of three-port converter and ESS, although involving the highest operation cost. Configuration D is the most expensive due to its installation features. Configuration B represents the most convenient choice in this analysis.

4.3. Optimal planning with minimum ESS installation

The application of minimum ESS installation constraint (11), properly tailored according to the results reported in Section 4.2 (requiring an I_{sto}^{min} of 3 kWh for Configurations A and C, 6 kWh for Configuration D and 10 kWh for Configuration B), leads to the results reported in Table 4.

It can be inferred that installation costs for Configurations A and C increase greatly with respect to the previous results, due to the addition of ESS and relevant converter. A further increase of installation cost is observed for Configuration D due to increased three-port converter size,

Table 6
Reliability indices for optimally sized DC microgrid configurations.

Condition	Quantity	Configuration A	B	C	D
Without minimum ESS installation	*EENS*	156.7	111.9	175.8	125.8
	EEND	38.9	18.4	45.9	15.6
With minimum ESS installation	*EENS*	59.5	91.1	112.2	110.0
	EEND	7.1	10.6	7.1	8.8

whereas the only additional battery module does not influence much Configuration B installation cost. As regards the operation, the presence of the first battery module in Configurations A and C remarkably affects the reduction of grid exchanges, whereas additional ESS modules in Configurations B and D are exploited to reduce EV discharge recourse.

4.4. Reliability analysis and configuration comparison

The analysis is based on the assessment of failure rates and availability of each device, and on their combination according to various DC microgrid configurations. The details of device-level assessment are illustrated in Appendix A, providing the values for the four converter types described in Section 2, and for PV system, ESS modules, external grid connection, AC and DC connectors.

In the analysed DC-microgrid configurations, numerous series connections of devices can be pointed out (e.g. for Configuration A, PV system and monodirectional DC/DC converter, as well as external grid and AC/DC converter). Therefore, equivalent devices are defined as the set of the devices in series, whose reliability parameters are obtained by applying (14.a)–(14.b) to the involved devices. The presence of equivalent devices in configurations along with their reliability features are reported in Table 5. It can be seen that Configurations A and B involve up to 8 equivalent devices, Configuration C up to 9 and Configuration D up to 10, since the three-port converter can work even if only one of connected sources is available, but its failure implies the unavailability of both connected devices. Therefore, up to 256, 256, 512 and 1024 availability states are analysed for the four configurations, respectively. In the absence of the installation of a device, e.g. Configuration A without minimum ESS, the number of states decrease.

The rule-based curtailment procedure with priority is therefore employed for each availability state. As regards success parameter π_σ for Configuration B in states with grid failure and ESS availability (see Table 2), it is supposed to increase by 1/25 for each kWh of installed ESS capacity, reaching the maximum value of 1 from 25 kWh to 60 kWh, representing the maximum expected installation for the final demonstrator, as reported in [50]. Whereas, for Configuration D, the failure of ESS and of either the external grid or the AC/DC bidirectional converter implies $\pi_\sigma = 0$.

By means of (17.a)–(17.b), the values of yearly *EENS* and *EEND* for the four configurations are evaluated, also in the presence of minimum ESS constraint, as reported in Table 6. It can be seen that, with the base formulation, Configuration B presents the lowest values of *EENS* and *EEND*, and Configuration D reaches analogous behaviour. Whereas, Configuration C shows the worst performance, and Configuration A is placed in the middle. With the minimum ESS installation constraint (19), a reduction of indices is obtained in all cases. In addition, Configuration A becomes the most indicated to improve reliability indices. Whereas, in Configuration D both indices do not experience remarkable changes with respect to the initial formulation.

Techno-economic planning and reliability indices are put in relation in the following Fig. 11, reporting *EENS* and *EEND* in percentage of the total EV charge and discharge, respectively, and total microgrid cost is reported in p.u. of the results of Configuration A without minimum ESS. In the Figure, values in the absence (w/o) and in the presence (with) of minimum ESS constraint are reported. It can be observed that, even though Configuration B shows lower costs, Configuration A with minimum ESS shows an advantage on *EENS* percentage level. Moreover, *EEND* percentage values are always lower than *EENS* ones. Considering *EEND* levels, Configurations A and C have analogous values, but the former is still preferable due to lower costs, whereas Configurations B and D show limited advantages from increased ESS installation.

Total microgrid investment, operation and reliability cost, obtained as the sum of C_T and C_R defined in (19) is determined in a range of *VOLL* between 0.1 €/kWh (for insensible loads) and 30 €/kWh (for extremely sensible loads) [51,52] in the analysed cases (four configurations with and without constraint (11)). Relevant trends are reported in Fig. 12, and it stems that reliability aspects involve a remarkable increase of total cost, between 20% and 70% at maximum *VOLL*. Without minimum ESS

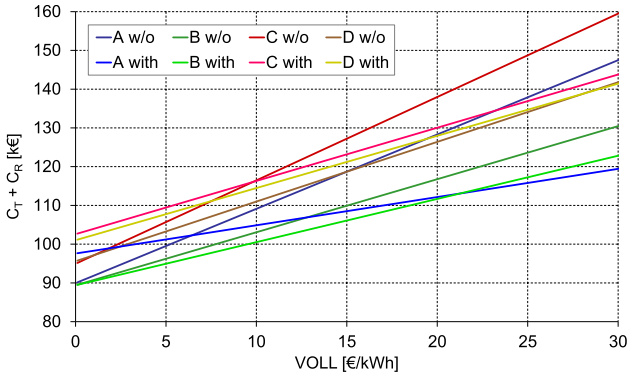

Fig. 12. Trends of microgrid installation, operation and reliability cost with varying VOLL.

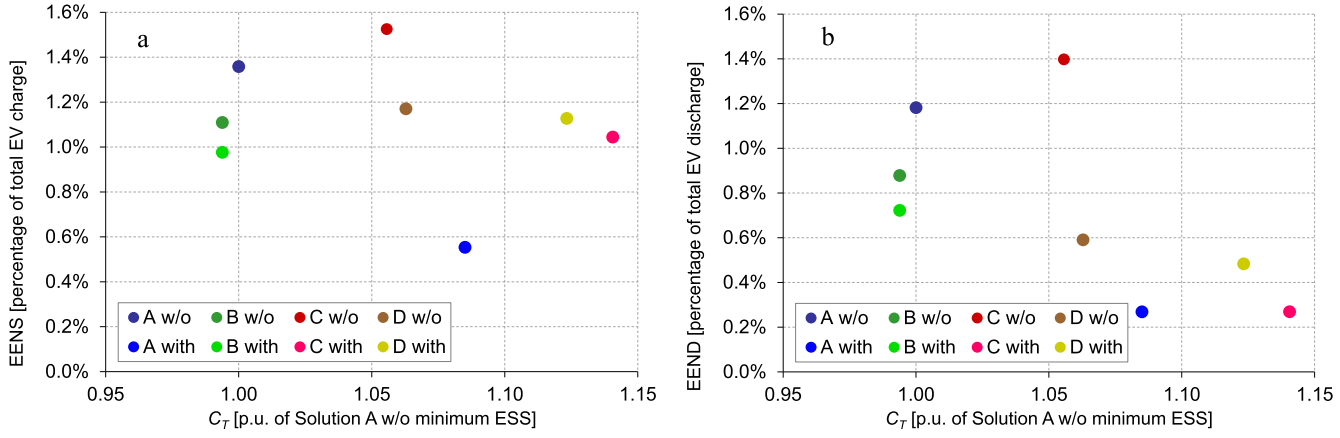

Fig. 11. Comparison of microgrid total cost with EENS (a) and EEND (b).

installation, Configuration B is always the most convenient, and Configuration D becomes preferable to Configuration C for *VOLL* = 2 €/kWh, whereas the breakeven with Configuration A is observed for *VOLL* = 15 €/kWh. With minimum ESS installation, all configurations show an increasing advantage as long as *VOLL* grows, and all of them result preferable to the corresponding case without minimum ESS from *VOLL* = 28 €/kWh. Around *VOLL* = 22 €/kWh, Configuration A with minimum ESS becomes more convenient than Configuration B with minimum ESS.

5. Conclusions

In this paper, a method to assess sizing, operation and reliability of four different configurations of a DC microgrid including PV, EV stations and energy storage, according to converter selection and connection, has been carried out. In particular, a mixed-integer linear optimization methodology for the techno-economic planning of the DC microgrid, based on the definition of operating scenarios, has been considered and tailored to the peculiar features of the inspected technical configurations. Furthermore, a reliability analysis has been described, in order to evaluate the amount of energy exchange with EVs that can be curtailed in the presence of device unavailability, by means of a rule-based redispatching with priority. The proposed approach has been applied to a case study of envisaged DC microgrid for a fleet of service EVs at Bari Port premises. Results have shown that the presence of ESS can be hindered by the higher cost due to dedicated converters, although it makes reliability performances increase, and the configuration with one converter per each source reveals the best compromise for sizing, operation and reliability costs. Future work will deal with the application of refined operation strategies, accounting for short-term source and EV variability, and for the provision of internal and grid services.

Funding

This document has been created in the context of the CONNECT project. The CONNECT project has received funding from the ECSEL Joint Undertaking under Grant Agreement n° 737434-2 and from the national programmes/funding authorities of Germany, Italy, Slovakia, Spain and The Netherlands. The ECSEL JU has no liability in respect of this document, which is merely representing the authors' view.

CRediT authorship contribution statement

B. Aluisio: Methodology, Software, Writing - original draft, Data curation, Visualization. **M. Dicorato:** Conceptualization, Investigation, Data curation, Validation, Writing - review & editing, Supervision, Project administration. **I. Ferrini:** Software, Data curation, Visualization. **G. Forte:** Methodology, Software, Formal analysis, Writing - original draft, Visualization. **R. Sbrizzai:** Conceptualization, Investigation, Data curation. **M. Trovato:** Methodology, Formal analysis, Validation, Writing - review & editing, Supervision.

Declaration of Competing Interest

The authors declare that they have no known competing financial interests or personal relationships that could have appeared to influence the work reported in this paper.

Appendix A. Determination of reliability characteristics of DC microgrid devices.

Reliability characteristics of the converters derive from a set of internal components (switches, diodes, inductors, capacitors), whose failure rates λ_q are derived from the data and methodology described in [53]. The application of (13)-(14) to the four converter topologies reported in Fig. 5–Fig. 8 is synthesized in Table A.1, along with proper repair rate and the determination of A_z and U_z. It is clear that the three-port converter implies the lowest reliability due to the highest number of components.

Reliability features of sources and other devices are reported in Table A.2. In particular, for PV panels data from [54] are exploited, including modules, by-pass diodes and connector pins. Moreover, strings with at most 12 modules in series, equipped with a fuse and disconnector, are considered, in order to reach a suitable output voltage level for the integration with converters, in the range of 500–600 V. For lithium-based battery modules, data from [55,56] are considered, and since a single module allows to obtain the desired output voltage, strings of modules are not necessary. External grid is supposed to be connected by means of a 500-m cable ending in a MV/LV transformer station with a single transformer, and relevant reliability data are taken from [57,58]. The estimation of failure rate and availability for DC and AC connectors is taken from [52,53].

For EV charging stations, reliability features correspond to those of bidirectional DC/DC converter, coherently with the assumption of fully available EVs [26].

Table A.1
Reliability characteristics of converters.

	Number of components $n_{q,z}$				Reliability characteristics			
Device	Switch	Diode	Inductor	Capacitor	λ_z [failure/h]	μ_z [repair/h]	A_z	U_z
DC/DC monodir.	1	1	1	1	$3.562{\cdot}10^{-6}$	$5.0{\cdot}10^{-3}$	0.99929	$7.119{\cdot}10^{-4}$
DC/DC bidir.	2	2	1	1	$7.117{\cdot}10^{-6}$	$5.0{\cdot}10^{-3}$	0.99858	$1.421{\cdot}10^{-3}$
AC/DC	6	6	0	0	$2.133{\cdot}10^{-5}$	$2.5{\cdot}10^{-3}$	0.99154	$8.460{\cdot}10^{-3}$
AC/DC/DC three-port	6	7	2	2	$2.138{\cdot}10^{-5}$	$2.0{\cdot}10^{-3}$	0.98942	$1.058{\cdot}10^{-2}$

Table A.2
Reliability features of modules, sources and devices

Device	λ_z [failure/h]	μ_z [repair/h]	A_z	U_z
PV system	$3.065{\cdot}10^{-5}$	$8.497{\cdot}10^{-3}$	0.99641	$3.594{\cdot}10^{-3}$
ESS LiPo module	$9.132{\cdot}10^{-6}$	$3.425{\cdot}10^{-3}$	0.99734	$2.660{\cdot}10^{-3}$
External grid	$4.110{\cdot}10^{-6}$	$5.708{\cdot}10^{-3}$	0.99928	$7.195{\cdot}10^{-4}$
AC connector	$3.800{\cdot}10^{-7}$	$2.000{\cdot}10^{-2}$	0.99998	$1.900{\cdot}10^{-5}$
DC connector	$6.960{\cdot}10^{-7}$	$2.778{\cdot}10^{-2}$	0.99997	$2.505{\cdot}10^{-5}$

References

[1] Kumar Panwar L, Srikanth Reddy K, Kumar R, Panigrahi BK, Vyas S. Strategic Energy Management (SEM) in a micro grid with modern grid interactive electric vehicle. Energy Convers Manage Dec. 2015;106:41–52.

[2] Aluisio B, Conserva A, Dicorato M, Forte G, Trovato M. Optimal operation planning of V2G-equipped Microgrid in the presence of EV aggregator. Electr Power Syst Res Nov. 2017;152:295–305.

[3] Shekari T, Golshavannaz S, Aminifar F. Techno-economic collaboration of PEV fleets in energy management of microgrids. IEEE Trans Power Syst Sept. 2017;32 (5). 3883-3841.

[4] Chandra Mouli GR, Bauer P, Zeman M. System design for a solar powered electric vehicle charging station for workplaces. Appl Energy April 2016;168:434–43.

[5] Fathabadi H. Novel solar powered electric vehicle charging station with the capability of vehicle-to-grid. Solar Energy Jan. 2017;142:136–43.

[6] Domínguez-Navarro JA, Dufo-López R, Yusta-Loyo JM, Artal-Sevil JS, Bernal-Agustín JL. Design of an electric vehicle fast-charging station with integration of renewable energy and storage systems. Int J Electr Power Energy Syst Feb. 2019; 105:46–58.

[7] Aluisio B, Dicorato M, Forte G, Trovato M. A Monte-Carlo Based procedure for optimal sizing of integrated Electric Vehicle Supply Infrastructure. In: Proc. of IEEE ISGT Europe 2017 Conference, 26-29 Sept. 2017, Turin, Italy, pp. 1-6.

[8] Hu K-W, Liaw C-M. Incorporated operation control of DC microgrid and electric vehicle. IEEE Trans Ind Electron Jan. 2016;63(1):202–15.

[9] Kaur S, Kaur T, Khanna R, Singh P. A state of the art of DC microgrids for electric vehicle charging. In: Proc. of 2017 ISPCC Conf., 21-23 Sept. 2017, Solan, India.

[10] Dragicevic T, Lu X, Vasquez J, Guerrero J. DC microgrids Part I: a review of control strategies and stabilization techniques. IEEE Trans Power Electron Jul. 2016;31(7): 4876–91.

[11] Aluisio B, Dicorato M, Ferrini I, Forte G, Trovato M. AC and DC solutions for Electric Vehicle microgrid: sizing and reliability analysis. In: Proc. of IEEE 2018 EEEIC/I&CPS Europe Int. Conf., 12-15 June 2018 Palermo, Italy, pp. 1-6.

[12] Dastgeer F, Gelani HE, Anees HM, Paracha ZJ, Kalam A. Analyses of efficiency/ energy-savings of DC power distribution systems/microgrids: past, present and future. Int J Electr Power Energy Syst Jan. 2019;104:89–100.

[13] Meng L, Shafiee Q, Trecate GF, Karimi H, Fulwani D, Lu X, et al. Review on control of DC microgrids and multiple microgrid clusters. IEEE J Emerg Sel Top Power Electron 2017;5(3):928–48.

[14] de Paula García-Lopez F, Barragán-Villarejo M, Maza-Ortega JM. Grid-friendly integration of electric vehicle fast charging station based on multiterminal DC link. Electrical Power and Energy Systems, vol. 114, Jan. 2020, paper n. 105341.

[15] Shi X, Bazzi AM. Reliability modeling and analysis of a micro-grid with significant clean energy penetration. In: Proc. of 9th International Conference on Power Electronics-ECCE Asia, June 1-5 2015, Seoul, South Korea, pp. 202-207.

[16] Adefrati T, Bansal RC. Reliability and economic assessment of a microgrid power system with the integration of renewable energy resources. Appl Energy 2017;206: 911–33.

[17] Lotfi H, Khodaei A. Hybrid AC/DC microgrid planning. Energy 2017;118:37–46.

[18] Baghaee HR, Mirsalim M, Gharehpetian GB, Talebi HA. Reliability/cost-based multi-objective Pareto optimal design of stand-alone wind/PV/FC generation microgrid system. Energy 2016;115:1022–41.

[19] Wang C, Jiao B, Guo L, Yuan K, Sun B. Optimal planning of stand-alone microgrids incorporating reliability. J Mod Power Syst Clean Energy 2014;2(3):195–205.

[20] Abdulkarim A, Abdelkader SM, Morrow DJ. Model for optimum design of standalone hybrid renewable energy microgrids. J Fundamental Appl Sci 2018;9 (2):1074–101.

[21] Moradi MH, Eskandari M, Mahdi Hosseinian S. Operational strategy optimization in an optimal sized smart microgrid. IEEE Trans Smart Grid 2015;6(3):1087–95.

[22] Fronda DC, Rosendo KTU, Pedrasa MAA. Optimization of isolated microgrids with cost and reliability targets. In: Proc. of IEEE 2017 ISGT-Asia Conference, 4-7 Dec. 2017, Auckland, New Zealand, pp. 1-6.

[23] Dominguez EX, Arboleya P. Reliability assessment in photovoltaic nanogrids by means of principal components analysis. In: Proc. of IEEE 2016 PES General Meeting, 17-21 July 2016, Boston, MA, USA, pp. 1-5.

[24] Bai H, Miao S, Zhang P, Bai Z. Reliability evaluation of a distribution network with microgrid based on a combined power generation system. Energies Feb. 2015;8(2): 1216–41.

[25] Linhao Y, Ke W, Xu C, Tingcheng H, Mengying L. Reliability Evaluation of microgrid considering electric vehicles and demand response. In: Proc. of Powercon 2018, 6-8 Nov. 2018, Guangzhou, China, pp. 1-5.

[26] Guner S, Ozdemir A. Reliability improvement of distribution system considering EV parking lots. Electric Power Syst Res Aug. 2020;185. paper n. 106353.

[27] Bin Irshad U, Nizami MSH, Rafique S, Hossain MJ, Mukhopadhyay SC. A battery energy storage sizing method for parking lot equipped with EV chargers. IEEE Syst J, in press.

[28] Dai Q, Liu J, Wei Q. Optimal photovoltaic/battery energy storage/electric vehicle charging station design based on multi-agent particle swarm optimization algorithm. Sustainability April-1 2019;11(7). paper n. 1973.

[29] Haupt L, Schöpf M, Wederhake L, Weibelzahl M. The influence of electric vehicle charging strategies on the sizing of electrical energy storage systems in charging hub microgrids. Appl Energy Sept. 2020;273. paper n. 115231.

[30] Liu G, Xue Y, Chinthavali MS, Tomsovic K. Optimal sizing of PV and energy storage in an electric vehicle extreme fast charging station. In: Proc. of 2020 IEEE ISGT Conference, Washington DC, U.S.A., 17-20 Feb. 2020, pp. 1-5.

[31] Safak Bayram I, Galloway S, Burt G. A probabilistic capacity planning methodology for plug-in electric vehicle charging lots with on-site energy storage systems. J Energy Storage Dec. 2020;32. paper n. 101730.

[32] Mehrjerdi H, Hemmati R. Electric vehicle charging station with multilevel charging infrastructure and hybrid solar-battery-diesel generation incorporating comfort of drivers. J Energy Storage Dec. 2019;26. paper n. 100924.

[33] Davidov S, Pantoš M. Optimization model for charging infrastructure planning with electric power system reliability check. Energy Jan. 2019;166:886–94.

[34] Wu X, Hu X, Teng Y, Qian S, Cheng R. Optimal integration of a hybrid solar-battery power source into smart home nanogrid with plug-in electric vehicle. J Power Sources Sept. 2017;363:277–83.

[35] Sadeghi D, Nasghshbandy AH, Bahramara S. Optimal sizing of hybrid renewable energy systems in presence of electric vehicles using multi-objective particle swarm optimization. Energy Oct. 2020;2019. paper n. 118471.

[36] Aluisio B, Dicorato M, Ferrini I, Forte G, Sbrizzai R, Trovato M. Optimal sizing procedure for electric vehicle supply infrastructure based on DC microgrid with station commitment. Energies May-2 2019;12(10). paper n. 1901.

[37] Dambone Sessa S, Chiarelli A, L'Abbate A, Benato R. Availability assessment methods for HVDC systems: a review. In: Proc. of AEIT HVDC 2019 Conference, Florence, Italy, 9-10 May 2019.

[38] Dragičević T, Lu X, Vasquez JC, Guerrero JM. DC Microgrids – Part II: a review of power architectures, applications, and standardization issues. IEEE Trans Power Electron 2016;31(5):3528–49.

[39] Bruni G, Cordiner S, Galeotti M, Mulone V, Nobile M, Rocco V. Control strategy influence on the efficiency of a hybrid photovoltaic-battery-fuel cell system distributed generation system for domestic applications. Energy Procedia, Vol. 45, 2014 (Proc. of ATI 2013 Conf.), pp. 237-246.

[40] Wang P, Jin C, Zhu D, Tang Y, Loh PC, Choo FH. Distributed control for autonomous operation of a three-port AC/DC/DS hybrid microgrid. IEEE Trans Ind Electron Febr. 2015;62(2):1279–90.

[41] Čepin M. Assessment of Power System Reliability – Methods and Applications. Springer; 2011.

[42] Aghdam FH, Abapour M. Reliability and cost analysis of multistage boost converters connected to PV panels. IEEE J Photovoltaics 2016;6(4):981–9.

[43] Ghavami M, Singh C. Reliability evaluation of plug-in hybrid electric vehicle chargers. In: Proc. of IEEE 2017 EEEIC/I&CPS Europe Int. Conf, 6-9 June 2017, Milan, Italy, pp. 1-5.

[44] Theristis M, Papazoglou IA. Markovian reliability analysis of standalone photovoltaic systems incorporating repairs. IEEE J Photovoltaics 2014;4(1): 414–22.

[45] Koh LH, Wang P, Choo FH, Tseng K-J, Gao ZY, Püttgen HB. Operational adequacy studies of a PV-based and energy storage stand-alone microgrid. IEEE Trans Power Syst 2015;30(2):892–900.

[46] Liu N, Zhou F, Wang L, Wang C, Chen Z, Chen Q. Online energy management of PV-assisted charging station under time-of-use pricing. Electr Power Syst Res 2016; 137:76–85.

[47] Ansari OA, Safari N, Chung CY. Reliability assessment of microgrid with renewable generation and prioritized loads. In: Proc. of 2016 IEEE Green Energy and Systems Conference, Long Beach, CA, USA, 6-7 Nov. 2016, pp. 1-6.

[48] Fathabadi H. Novel high efficiency DC/DC boost converter for using in photovoltaic systems. Sol Energy Feb. 2016;125:22–31.

[49] Shu X, Yang W, Guo Y, Wei K, Qin B, Zhu C. A reliability study of electric vehicle battery from the perspective of power supply system. J Power Sources March 2020; 451. paper n. 227805.

[50] Dicorato M, Forte G, Trovato M, Boigues Muñoz C, Coppola G. An integrated DC microgrid solution for electric vehicle fleet management. IEEE Trans Ind Appl Nov.-Dec. 2019;55(6):7347–55.

[51] Vahedipour-Dahraie M, Anvari-Moghaddam A, Guerrero JM. Evaluation of reliability in risk-constrained scheduling of autonomous microgrids with demand response and renewable resources. IET Renew Power Gener 2018;12(6):657–67.

[52] Lombardi P, Styczynski Z, Sokolnikova T, Suslov K. Use of energy storage in isolated micro grids. In: Proc. of 2014 PSCC Conference, 18-22 Aug. 2014, Wroclaw, Poland, pp. 1-6.

[53] Military Handbook MIL-HDBK-217F Notice 2. "Reliability Prediction of Electronic Equipment. U.S. Department of Defense; 1995.

[54] Colli A. Failure mode and effect analysis for photovoltaic systems. Renew Sust Energy Rev Oct. 2015;50:804–9.

[55] Mukherjee N, Strickland D. Second life battery energy storage systems: converter topology and redundancy selection. In: Proc. of 7th IET PEMD Conference, 8-10 Apr. 2014, Manchester, UK, pp. 1-6.

[56] Chatzinikolaou E, Rogers DJ. A comparison of grid-connected battery energy storage system designs. IEEE Trans Power Electron Sept. 2017;32(9):6913–23.

[57] Costa PM, Matos MA. Assessing the contribution of microgrids to the reliability of distribution networks. Electr Power Syst Res Feb. 2009;79(2):382–9.

[58] Jürgensen JH, Nordström L, Hilber P. Individual failure rates for transformers within a population based on diagnostic measures. Electr Power Syst Res Dec. 2016;141:354–62.